An electrode design study: laser structuring of anodes for fast-charging of batteries

Y. Sterzl*, W. Pfleging
Institute for Applied Materials (IAM-AWP), Karlsruhe Institute of Technology, P.O. Box 3640, 76021 Karlsruhe, Germany

ABSTRACT

Graphite anodes with high areal loading of 3.6 mAh cm^{-2} were laser structured with various design patterns using an ultrashort pulsed laser system of high average power (>300 W). The upscaling potential of the most common pattern types in literature, namely the line, grid, and hexagonal hole pattern were evaluated and the influence of process parameters like laser fluence and repetition rate on the ablation characteristics were examined. The fast-charging capability of full-cells containing structured graphite anodes were studied with NMC622 cathodes. For each structure pattern the onset of lithium plating during fast-charging was determined by differential voltage analysis of the voltage relaxation.

Keywords: ultrashort pulsed laser ablation, fast charging, graphite, lithium-ion battery, 3D battery, upscaling, electrode structuring

1. INTRODUCTION

The ongoing development of lithium-ion batteries has offered a way to solve the problems of increasing electrification, especially in the transport sector. The use of active materials with high specific capacitance, but also the implementation of thick-film electrodes, with film thicknesses of 100 µm and higher, lead to the high energy densities (550 Wh l^{-1}) achievable today in commercial LIBs [1]. With driving ranges of up to 500 km, battery electric vehicles (BEVs) already reach similar ranges compared to vehicles with internal combustion engines [2]. However, recharging BEVs within comparable times to refueling cars with internal combustion engines is still a challenge [3]. The degradation of the battery associated with fast-charging, such as lithium plating, leads to irreversible loss of capacity and causes a safety risk [4]. Several ways of modifying the electrode architecture to increase fast-charging capability are contrary to current research. For instance, multilayer coating, blending of different active materials, and structuring of the electrode with laser ablation are being investigated and show an increase in fast-charging capabilities [5-11]. Several patterns for laser structuring, including hole, line, and grid patterns are investigated in the literature [8, 10, 12].

Habedank et al. [13]] structured a hexagonal arranged hole pattern into 70 µm thick graphite electrodes with a pulsed Nd:YAG fiber laser operating at a pulse length of 150 ps and a repetition rate of 1.2 MHz. Full-cells with NMC111 cathodes and a capacity loading of 2.75 mAh cm^{-2} showed reduced lithium plating at low temperatures of down to -15 °C and C-rates of up to 2C. Cells with structured electrodes showed very low lithium plating at temperatures of 0 °C, whereas the unstructured reference cells showed significant degradation due to lithium plating. The authors attributed the higher fast-charging capacity and the shifted onset of lithium plating to higher C-rates to the enhanced diffusion kinetics in structured electrodes.

Zheng et al. [14] investigated the fast-charging capability of structured graphite and silicon/graphite electrodes with line and grid patterns. Half-cells with structured electrodes with a thickness of 75 µm (graphite) and 55 µm (silicon/graphite) reached higher charging capacities at C-rates ≥ C/2 compared to cells with the unstructured reference electrode. Furthermore, post-mortem analyses showed significantly reduced or no crack formation of the coating caused by the volume expansion of silicon and graphite in laser structured electrodes.

In the study presented, the laser structuring of hole, line, and grid patterns in graphite electrodes, as well as the fast-charging capability of structured electrodes with these pattern types, is investigated. Particular attention was paid to the mass loss due to structuring and the resulting cell balancing of the cells with structured and unstructured electrodes, as well as the lithium plating due to fast charging as a function of pattern type.

2. METHODOLOGY

2.1 Electrode manufacturing

For the preparation of the anodes, a water-based 2 wt.% sodium carboxymethyl cellulose solution (CMC, MTI Corporation, USA) was prepared using a dissolver (Labordissolver DB13, DISTECH GmbH, Germany). Subsequently, graphite (SPGPT808, Targray Inc., Canada) and carbon black (CB, Timcal Super C65, MTI Corporation, USA) were added to the CMC solution and mixed with a centrifugal mixer (Speedmixer DAC 150 SP, Hauschild, Germany). After homogenizing the mixture, a styrene butadiene rubber solution (SBR, 50 wt.% solid content, MTI Corporation, Richmond, CA, USA) was stirred into the graphite, carbon black, and CMC solution at a low rotational speed. The resulting anode slurry was doctor blade coated onto 9 µm thick copper foil and dried at ambient conditions before the electrodes were calandered to a porosity of 40 %. To compensate the mass loss of the later laser structuring, two electrodes with different areal capacities were produced. For the preparation of the cathodes, NMC622 (BASF, Germany) was mixed with conductive graphite and carbon black (C-nergy Super C65, Imerys G&C, Switzerland) in an N-methyl-2-pyrrolidone (NMP, Merck KGaA, Germany) based polyvinylidene fluoride (PVDF, Solef® 5130, Solvay Specialty Polymers, France) solution with a weight proportion of 1:10 using a centrifugal mixer. The cathode slurry was doctor blade coated onto 20 µm thick aluminum foil and dried for 3 h at 90 °C before the electrodes were calandered to a porosity of 35 %.

Table 1: Composition, porosity and areal capacity of the built electrodes

Material	Anode slurry	Cathode slurry
Graphite	93	-
CB	1.4	3
CMC	1.87	-
SBR	3.73	-
NMC622	-	92
PVDF	-	3
conductive graphite	-	2
Areal capacity	3.62 mAh cm^{-2} / 3.18 mAh cm^{-2}	2.55 mAh cm^{-2}

2.2 Laser structuring

A high-power, high repetition rate laser source (FX600-2-GFH, EdgeWave GmbH, Germany) implemented in a laser micromachining system (MSV203 Laser Patterning Tool, M-SOLV LTD, UK) was used to structure the calandered anodes with an areal capacity of 3.62 mAh cm^{-2}. The laser operating at a wavelength of 1030 nm, had a maximum average power of 300 W at a repetition rate of 1.5 MHz. The calculated beam radius at the focus is 24 µm. The line pattern was structured with an average laser power of 40 W, a repetition rate of 1.5 MHz, a scanning speed of 20 m s^{-1}, and a sufficient number of passes to ablate down to the current collector. The pitch for the line pattern was set to 300 µm. For the grid pattern, the repetition rate, the average laser power, and the scanning speed were decreased by a factor of 10 to account for the higher complexity of the structure pattern. The pitch for the grid pattern was set to 580 µm to achieve comparable mass losses. The hole pattern was structured using a repetition rate of 100 kHz, an average laser power of 7 W and a scanning speed of 13.5 m s^{-1}. With that, the hole-to-hole distance of 135 µm was adjusted by the scanning speed and repetition rate, and the ablation down to the current collector was ensured by a sufficient number of line scans. The laser structured anodes were examined regarding debris formation as well as mechanical and thermal induced damage with a digital microscope (VHX7000, Keyence, Japan).

2.3 Cell assembly and electrochemical testing

Anodes and cathodes with a diameter of 15 mm and 12 mm, respectively, were dried for 20 hours in a vacuum oven at 100 °C. CR2032 coin cells were assembled in an argon-filled glove box (LAB master pro sp, M. Braun Intergas-Systeme GmbH, Garching, Germany). A cell was constructed of one anode and one cathode, 160 µL of electrolyte (1.3 M LiPF6 ethylene carbonate and ethyl methyl carbonate (EC/EMC 3:7) with 5 wt.% FEC additive) and a polypropylene separator (Celgard LLC., USA). After cell assembly, the cells were stored for 20 h to ensure complete wetting of the components with electrolyte prior to electrochemical priming. The formation of the cells consisted of 3 cycles of constant current (CC)

with subsequent constant voltage (CV) charging and CC discharging at C/20 and a cut-off current equal to C/50 in a voltage window of 3 V-4.2 V. Subsequently, the cells were analyzed in a rate capability test as listed in Table 2. Between each charging and discharging step a rest period of 15 min was introduced, and for the last cycle at each C-rate a rest period of 4 h was applied to examine the voltage relaxation after fast-charging. In addition to the current limitation (Table 2), the CV phase was also limited by time (15 min) for the fifth cycle of each C-rate measurement. The capacity to calculate the C-rate was based on discharge capacity in the third formation cycle. The state-of-charge (SOC) was calculated with the mean charge capacity at 0.2C as reference.

Table 2: CCCV protocol of the rate capability test

Charging CC	0.1 C	0.2 C	0.5 C	1 C	2 C	3 C	5 C
Cut-off CV	0.05 C	0.1 C	0.1 C	0.1 C	0.1 C	0.1 C	0.1 C
Discharge CC	0.1 C	0.2 C	0.2 C	0.2 C	0.2 C	0.2 C	0.2 C
Repetitions	5	5	5	5	5	5	5

3. RESULTS AND DISCUSSION

3.1 Electrode structuring and cell characterization

Figure 1 shows digital microscope images of the structured electrodes with hole (a) grid (b) and line (c) pattern. For none of the investigated structure patterns, visible debris on the surface, or modifications of the current collector have been found. Due to the fact that the mass loss is dependent on the structure geometry and the structure pitch, the pitch was adjusted for each structure type to keep the mass loss comparable [15]. The mass loss was measured to 7.7 %, 8.1 %, and 8.0 % for the hole (Figure 1 (a); 135 µm pitch), grid (Figure 1 (b); 580 µm pitch), and line (Figure 1 (c); 300 µm pitch) structure, respectively, indicating well-chosen structuring parameters. The resulting areal capacity for the structured electrodes of each pattern type is 3.3 mAh cm^{-2} and is therefore slightly higher than for the unstructured reference electrode with an areal capacity of 3.2 mAh cm^{-2}. Due to an areal capacity of 2.55 mAh cm^{-2} for the cathodes, the N/P ratio of the built full-cells is 1.2-1.3 and the cell capacities are in the range of 2.88 mAh.

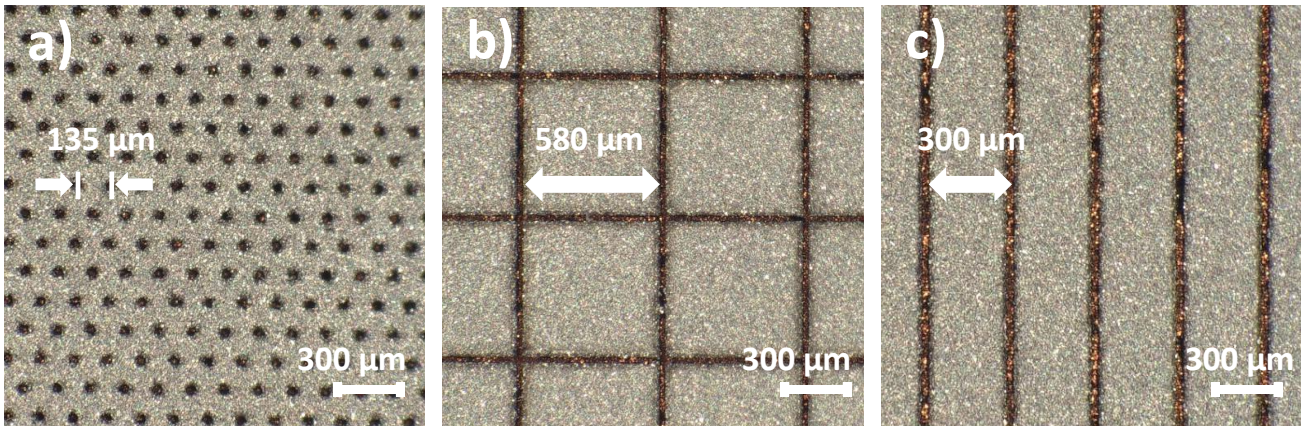

Figure 1: Digital microscope images of the laser structured electrodes with hole (a), grid (b) and line (c) pattern.

In Figure 2 the ablation depth is plotted as a function of the peak fluence for a constant number of passes (n=5) to illustrate the differences between the hole and the line ablation. The gray shading marks the area of the current collector for the used graphite electrode with the same composition and porosity as described in section 2.1 but with a reduced coating thickness of 55 µm. As one can see, the ablation depth increases with increasing peak fluence for the ablation of holes and grooves, which is already known in literature [9, 16]. Comparing the ablation depth of grooves and holes at the same peak fluence and number of passes, the reached ablation depth is higher for the generation of grooves. Thus, the current collector can be reached with five passes at a pulse peak fluence of 29.5J cm^{-2} for groove patterning, while only an ablation depth of 23 µm is reached for patterning of holes. The reason for this is attributed to the pulse overlap during laser ablation for generating grooves (pulse-to-pulse distance of 13.33 µm), which locally increases the number of pulses ablating the electrode. Line structures are therefore preferable to hole structures as they are more efficient in terms of ablation and have advantages in terms of the achievable processing speed due to the lower number of passes required for achieving the same ablation depth.

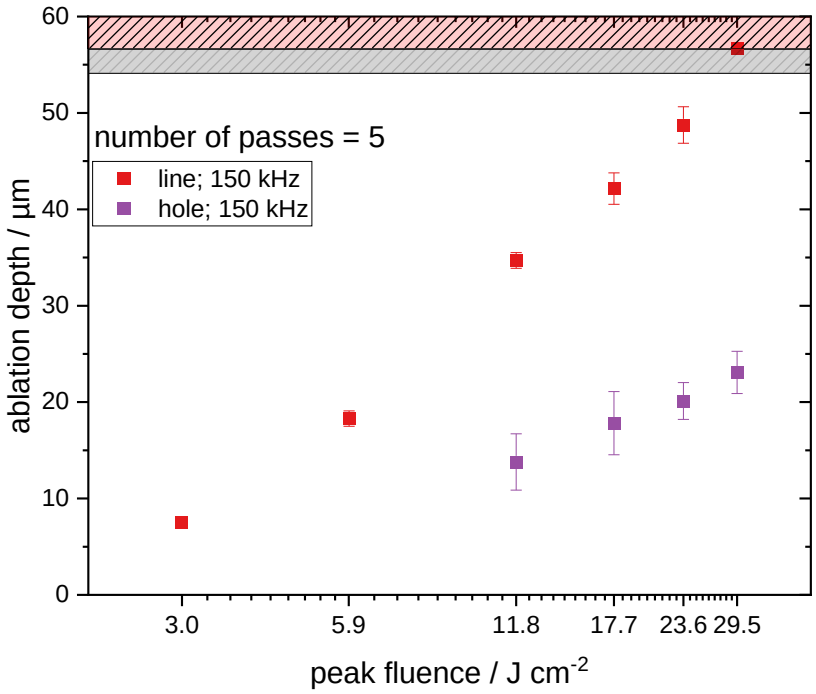

Figure 2: Ablation depth as a function of peak fluence for the patterning of holes (repetition rate of 150 kHz and laser scanning speed of 10 m s^{-1}) and the generation of lines (repetition rate 150 kHz and laser scanning speed of 2 m s^{-1}).

3.2 Fast-charging capability as a function of structure pattern

Figure 3 shows the reached SOC as a function of the C-rate after the CC (light colored) and CCCV (dark colored) charging phase in the fifth cycle of the respective C-rate (CV-phase limited to 15 min). For a clearer oversight, the maximum possible charging time is shown at the top of Figure 3, which decreases from 315 min at 0.2C to 27 min at 5C. A decrease in SOC after CCCV charging can be observed for cells with hole structured electrodes and cells with unstructured reference electrodes. The CCCV SOC declines from 100 % at 0.2C to 60 % and 52 % for the cells with hole structured electrodes and the reference cells, respectively. In contrast, the cells with line and grid structured electrodes remained a CCCV SOC of 92 % and 90 % at a C-rate of 5C. While a significant decrease in SOC in the CCCV phase is only observed for cells with hole and unstructured electrodes, a decrease in SOC in the CC phase is observed for all studied types of cells. The drop in reached SOC in the CC phase starts for all cells at a C-rate of 2C but is less pronounced for cells with line and grid

structured electrodes. This is particularly evident at the highest investigated C-rate of 5C, where a CC SOC of 50 % and 47 % can be achieved for cells with line and grid structured electrodes and only 7% and 4% for the cells with hole structured electrodes and the unstructured reference cells. Figure 3 also shows that an SOC of 80%, which is often set as a condition for fast-charging, can only be achieved for cells with line and grid-structured electrodes at high C-rates of up to 5C. The cells with hole-structured electrodes and the unstructured reference cells only achieve this SOC up to a C-rate of 2C.

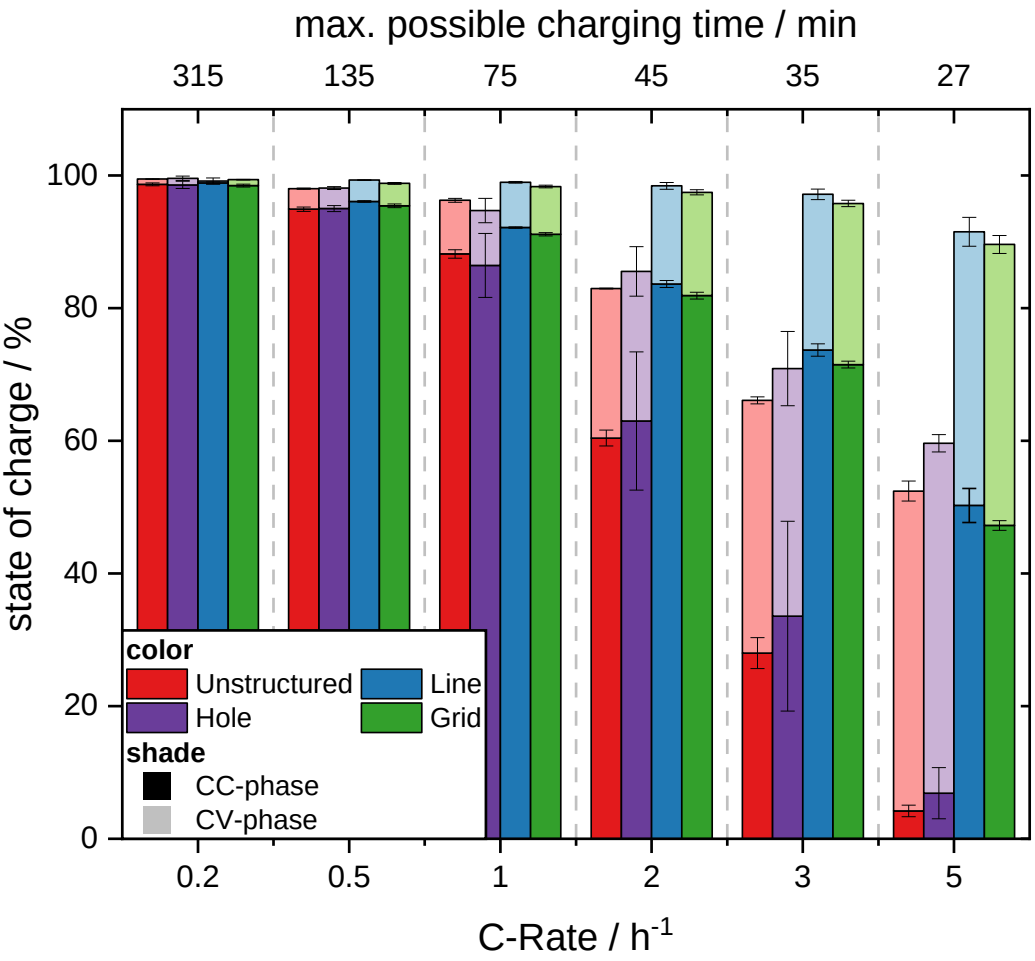

Figure 3: Gained SOC after CC and CCCV phase of charging for cells with line, grid, and hole structured electrodes as well as the unstructured reference.

The SOC achieved after charging is not the only criterion for evaluating the fast-charging capability of a battery. The absence of lithium plating during fast-charging must also be taken into account, as this represents a safety risk [4]. The voltage relaxation after fast-charging can be used to detect the onset of lithium plating [13, 17, 18]. The balancing of concentration gradients in the active material and electrode, as well as the reintercalation of plated lithium, leads to a characteristic voltage drop after charging with a plateau in the voltage transient [17]. The plateau in the voltage transient in the rest phase appears as a peak in the differential voltage analysis (dV/dt). Figure 4 shows the voltage relaxation over time (dotted line) and the dV/dt over time (solid line) for all studied structure types and the unstructured reference. For high charging C-Rates of up to 3C no peak in the dV/dt analysis can be observed for the cells with line structured electrodes or the cells with grid structured electrodes. In contrast, lithium plating starts at a C-rate of 2C in the unstructured cell and at 3C in the hole-structured cell, as can be seen from a plateau in the voltage relaxation and the corresponding peak in the

dV/dt. This results in a maximum C-rate for fast-charging of 1C for cells with unstructured electrodes, 2C for cells with hole structured electrodes and at least 3C for cells with line and grid structured electrodes. A shift in the onset of lithium plating to higher C rates in cells with structured electrodes is also reported in literature and is attributed to the enhanced diffusion kinetics in batteries assembled with structured electrode [8, 13].

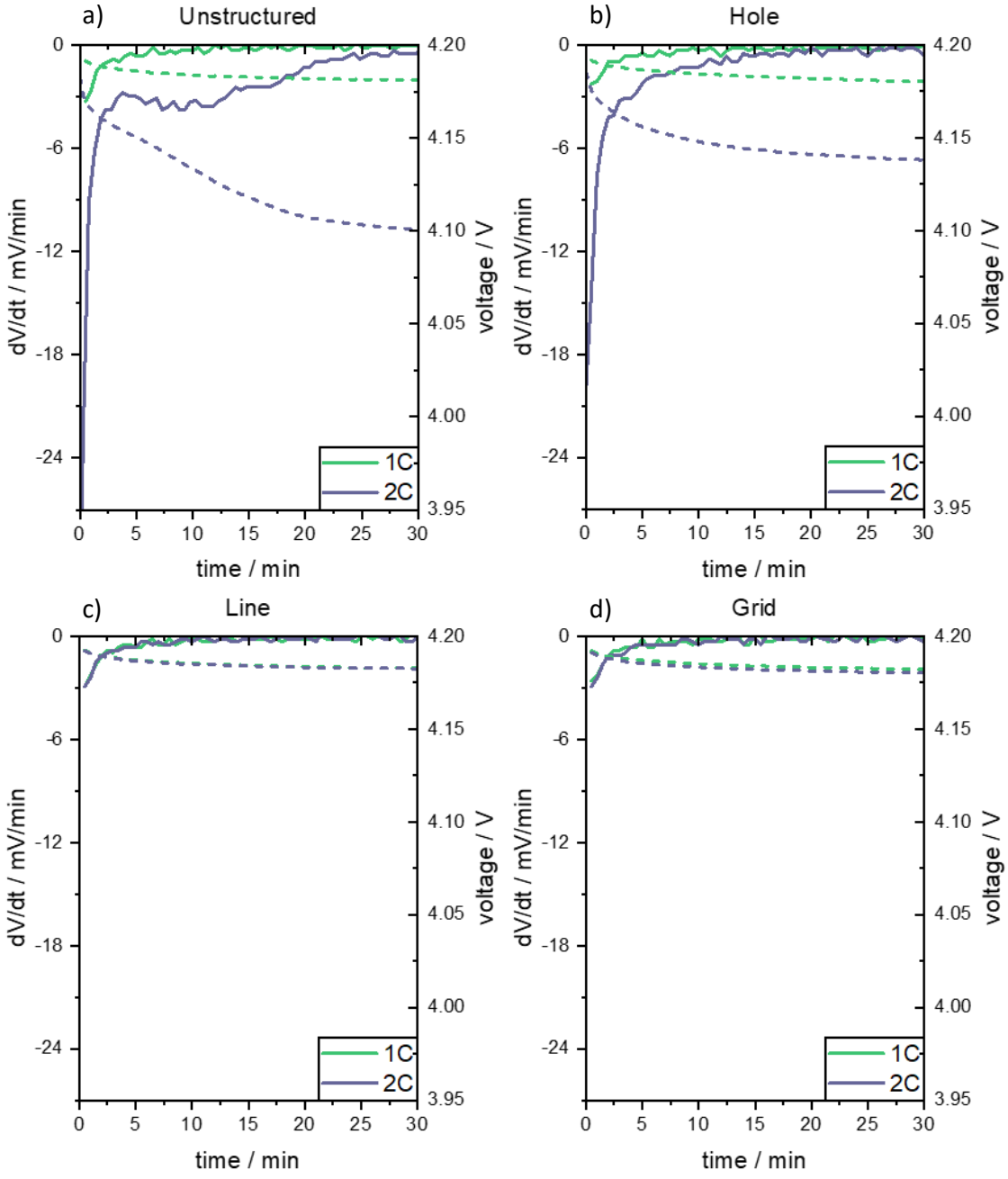

Figure 4: The dV/dt (solid) and the voltage relaxation (dotted) as a function of time for the reference (a) hole (b), line (c) and grid (d) structured cells.

4. CONCLUSION

In the presented study, the impact of the pattern type of anodes for lithium-ion batteries on the processability and fast-charging capability was systematically investigated. The use of ultrashort pulsed laser radiation with average power up to 300 W and repetition rates in the MHz regime was evaluated regarding the processing strategy and upscaling issues. Graphite anodes with high areal loading of 3.6 mAh cm^{-2} were patterned with the three most common structure types in literature, namely the line, grid, and hexagonal hole pattern. Process parameters like fluence, pulse overlap, and repetition rate were evaluated regarding an upscaling in a roll-to-roll environment for each pattern type and the generated structures were examined by digital microscopy. The mass loss of the patterned electrodes was limited to 8 % and the fast-charging capability of the structured and unstructured reference electrodes with similar loading was examined in full-cells with NMC622 cathodes. Furthermore, the onset of lithium plating for each structure pattern was determined by differential voltage analysis of the voltage relaxation after fast charging. It was shown that line and grid structures have advantages over hole structured electrodes in terms of processing, fast-charging capability, and onset of lithium plating. Thus, with the same peak fluence and number of passes, greater ablation depths are achieved when in the generation of grooves compared to generation of holes. Fast-charging of cells with unstructured electrodes (areal capacity 3.2 mAh cm^{-2}) is possible without lithium plating at C-rates of up to 1C. For cells with hole structured electrodes, the onset of lithium plating could be shifted to 3C and for cells with line and grid patterned electrodes, no lithium plating could be observed in the dV/dt even at C-rates of 3C.

5. ACKNOWLEDGEMENTS

We are grateful to our colleagues Marek Kapitz and Alexandra Reif for their support during laser processing and analytics. This project has received funding from the German Research Foundation (DFG, project No. 467624762)

6. REFERENCES

[1] S. Link, C. Neef, and T. Wicke, “Trends in Automotive Battery Cell Design: A Statistical Analysis of Empirical Data,” Batteries, 9(5), (2023).

[2] X. Shi, J. Pan, H. Wang *et al.*, “Battery electric vehicles: What is the minimum range required?,” Energy, 166, 352-358 (2019).

[3] M. Weiss, R. Ruess, J. Kasnatscheew *et al.*, “Fast Charging of Lithium-Ion Batteries: A Review of Materials Aspects,” Advanced Energy Materials, 11(33), (2021).

[4] T. Waldmann, B.-I. Hogg, and M. Wohlfahrt-Mehrens, “Li plating as unwanted side reaction in commercial Li-ion cells – A review,” Journal of Power Sources, 384, 107-124 (2018).

[5] K. H. Chen, V. Goel, M. J. Namkoong *et al.*, “Enabling 6C Fast Charging of Li-Ion Batteries with Graphite/Hard Carbon Hybrid Anodes,” Advanced Energy Materials, 11(5), (2020).

[6] L. Gottschalk, C. Oertel, N. Strzelczyk *et al.*, “Improving the Performance of Lithium-Ion Batteries Using a Two-Layer, Hard Carbon-Containing Silicon Anode for Use in High-Energy Electrodes,” Energy Technology, 11(5), (2022).

[7] D. Müller, A. Fill, and K. P. Birke, “Cycling of Double-Layered Graphite Anodes in Pouch-Cells,” Batteries, 8(3), (2022).

[8] K.-H. Chen, M. J. Namkoong, V. Goel *et al.*, “Efficient fast-charging of lithium-ion batteries enabled by laser-patterned three-dimensional graphite anode architectures,” Journal of Power Sources, 471, (2020).

[9] J. B. Habedank, J. Endres, P. Schmitz *et al.*, “Femtosecond laser structuring of graphite anodes for improved lithium-ion batteries: Ablation characteristics and process design,” Journal of Laser Applications, 30(3), (2018).

[10] Y. Zheng, D. Yin, H. J. Seifert *et al.*, “Investigation of Fast-Charging and Degradation Processes in 3D Silicon-Graphite Anodes,” Nanomaterials (Basel), 12(1), (2021).
[11] Y. Zheng, L. Pfäffl, H. J. Seifert *et al.*, “Lithium Distribution in Structured Graphite Anodes Investigated by Laser-Induced Breakdown Spectroscopy,” Applied Sciences, 9(20), (2019).
[12] A. Meyer, F. Ball, and W. Pfleging, “The Effect of Silicon Grade and Electrode Architecture on the Performance of Advanced Anodes for Next Generation Lithium-Ion Cells,” Nanomaterials (Basel), 11(12), (2021).
[13] J. B. Habedank, J. Kriegler, and M. F. Zaeh, “Enhanced Fast Charging and Reduced Lithium-Plating by Laser-Structured Anodes for Lithium-Ion Batteries,” Journal of The Electrochemical Society, 166(16), A3940-A3949 (2019).
[14] Y. Zheng, H. J. Seifert, H. Shi *et al.*, “3D silicon/graphite composite electrodes for high-energy lithium-ion batteries,” Electrochimica Acta, 317, 502-508 (2019).
[15] Y. Sterzl, and W. Pfleging, “Extending the 3D-battery concept: large areal ultrashort pulsed laser structuring of multilayered electrode coatings,” Proc. of SPIE 12409, 9 (2023).
[16] A. Meyer, Y. Sterzl, and W. Pfleging, “High repetition ultrafast laser ablation of graphite and silicon/graphite composite electrodes for lithium-ion batteries,” Journal of Laser Applications, 35(4), (2023).
[17] C. Uhlmann, J. Illig, M. Ender *et al.*, “In situ detection of lithium metal plating on graphite in experimental cells,” Journal of Power Sources, 279, 428-438 (2015).
[18] Y. Chen, K.-H. Chen, A. J. Sanchez *et al.*, “Operando video microscopy of Li plating and re-intercalation on graphite anodes during fast charging,” Journal of Materials Chemistry A, 9(41), 23522-23536 (2021).